processes

MDPI

Article

Evaluation of Antifungal Activity by Mixed Oxide Metallic Nanocomposite against *Candida* spp.

Ayodeji Precious Ayanwale, Brenda Lizbeth Estrada-Capetillo and Simón Yobanny Reyes-López *

Instituto de Ciencias Biomédicas, Universidad Autónoma de Ciudad Juárez, Envolvente del PRONAF y Estocolmo s/n, Ciudad Juárez 32300, Chih., Mexico; al171975@alumnos.uacj.mx (A.P.A.); lizbeth.capetillo@uacj.mx (B.L.E.-C.)
* Correspondence: simon.reyes@uacj.mx

Abstract: High doses of antimicrobial agents are a huge threat due to the increasing number of pathogenic organisms that are becoming resistant to antimicrobial agents. This resistance has led to a search for alternatives. Therefore, this study presents the synthesis and characterization of ZrO_2-Ag_2O nanoparticles (NPs) by sol-gel. The NPs were analyzed by dynamic light scattering (DLS), UV-visible (UV-vis), Raman and scanning electron microscopy (SEM). The NPs were later evaluated for their antifungal effects against *Candida albicans*, *Candida dubliniensis*, *Candida glabrata*, and *Candida tropicalis*, using disc diffusion and microdilution methods, followed by the viability study. The DLS showed sizes for ZrO_2 76 nm, Ag_2O 50 nm, and ZrO_2-Ag_2O samples between 14 and 42 nm. UV-vis shows an absorption peak at 300 nm for ZrO_2 and a broadband for Ag_2O NPs. Raman spectra were consistent with factor group analysis predictions. SEM showed spherically shaped NPs. The antifungal activity result suggested that ZrO_2-Ag_2O NPs were effective against *Candida* spp. From the viability study, there was no significance difference in viability as a function of time and concentration on human mononuclear cells. This promising result can contribute toward the development of alternative therapies to treat fungal diseases in humans.

Keywords: antifungal activities; ZrO_2-Ag_2O nanoparticles; mixed metal oxide; *Candida* spp.

Citation: Ayanwale, A.P.; Estrada-Capetillo, B.L.; Reyes-López, S.Y. Evaluation of Antifungal Activity by Mixed Oxide Metallic Nanocomposite against *Candida* spp. *Processes* **2021**, *9*, 773. https://doi.org/10.3390/pr9050773

Academic Editors: Yuan-Chang Liang and Sechul Chun

Received: 28 February 2021
Accepted: 18 April 2021
Published: 28 April 2021

1. Introduction

The death rate from fungal-related infections is worrisome, and in a population of immunocompromised individuals, fungal infections can contribute toward an increase in the morbidity and mortality rates [1]. *Candida* is a yeast that maintains a commensal relationship with the human body under normal circumstances [2], but in a situation where an individual has a compromised immune system, it becomes pathogenic [3], and may be the cause of oral and vaginal candidiasis, among other infections [4]. With a mortality rate of about 45%, the National Nosocomial Infections Surveillance System (NNISS, Atlanta, GA, USA) considers *Candida* as the fourth most prevalent nosocomial blood pathogen [1]. The resistance of *Candida* spp. to antifungal agents, such as fluconazole, flucytosine, amphotericin B, and echinocandins [5], due to reduction in membrane permeability to these agents, has fueled strong interest in the search for compounds with improved antifungal efficacies that have little or no cytotoxic implications [6]. In addition to antifungal resistance in *Candida* spp., commercial antifungal agents are reported to have one or more shortcomings in clinical applications, as seen with amphotericin B, which has bad effects on the kidney, resulting in renal failure, while fluconazole and the azoles family lead to complications that cause liver toxicity and the inhibition of testosterone synthesis [6]. Nanoparticles are known for their numerous applications in different fields, because they are not limited in function by their small size or morphology [7]. As seen in previous literature, nanoparticles are worthy alternatives as regards to combating fungal resistance to antifungal agents [8]. Different metal and metal oxide nanoparticles, such as silver nanoparticles, were researched extensively for their antimicrobial activities [9,10].

Nanocompounds of silver-containing materials are some of the most used commercial nanoparticles because of their strong toxicity toward fungi, bacteria, and viruses. This toxicity to microbes has favored their applications in personal care products, ointments, dressings as treatment for external wounds, and as resource material in surgical instruments. One major advantage of silver nanocompounds over other metal is due to their extremely potent antimicrobial characteristics. Silver nanoparticles are characterized by broad-spectrum antimicrobial activities that are effective against antibiotic-resistant strains. The effectiveness of silver nanoparticles as antimicrobial agents depend on the size and concentration of the nanoparticles. The smaller the size of the silver nanoparticle, the higher the antimicrobial activity when compared to larger nanoparticles. In nanoparticles of smaller sizes, the atoms are available at higher concentrations on the surface, and they have large surface area to volume ratios and, as such, exhibit more potent antimicrobial activity [11].

ZrO_2 nanoparticles are of great interest due to their scientific and technological applications in different fields, as well as their mechanical properties, electrical properties, wide band gaps, and high dielectric constants. Recently, there have been studies on nanocrystalline zirconia, as opposed to studies on their mechanical and electronic properties, mainly in microcrystalline zirconia (which was done in the past). From previous literature, zirconia nanoparticles have been synthesized by different physicochemical methods, such as the precipitation method, hydrothermal method, sol-gel method, and thermal decomposition; each of these methods determined the properties of the synthesized nanoparticles, as well as their applications as solid fuel cells, catalytic agents, gas sensors, or as high durability coatings [12]. Unlike silver nanoparticles, very little has been researched or reported on the antimicrobial activities of zirconium oxide nanoparticles, despite various reports claiming that zirconium oxide nanoparticles are stable and non-toxic [13]. To maximize the antimicrobial potential of silver oxide nanoparticles, there is a need to take the individual advantage of silver oxide nanoparticles, and complement with another metal oxide to form mixed metal oxide nanoparticles [14].

There has been a limited amount of studies published on the antifungal activities of silver and silver-containing compound nanoparticles [15]. In recent years, many researchers have reported on different antifungal agents. As early as 2019, Perween et al. reported the synthesis of silver nanoparticles as an upcoming therapeutic agent for resistant *Candida* infections. Though, it was concluded that silver nanoparticles could serve as new therapeutic agents for treating candidiasis, because of their considerable antifungal activities, emphasis was made on the need to improve the stability and to carry out further investigations on the toxic nature of silver nanoparticles [6]. Therefore, this study investigated the antimycotic effects of ZrO_2 and Ag_2O nanoparticles against selected pathogenic *Candida* species causing life-threatening fungal infections in humans. We also evaluated the changes in the antimycotic activity of Ag_2O on stabilizing with ZrO_2 nanoparticles.

2. Materials and Methods

2.1. Materials

Solvents used in the experiment were acetic acid and deionized water. Zirconium butoxide, ethylene glycol, silver nitrate, and citric acid were purchased from Sigma-Aldrich (St. Louis, MO, USA). The antifungal test was conducted using Sabouraud Dextrose Agar plates. All reactants used were of analytical grade and were used as received. Four candida species (*Candida albicans* ATCC MYA-2876, *Candida dubliniensis* ATCC MYA-580, *Candida glabrata* 2001, *and Candida tropicalis* 750) used in this study, were derived from American Type Culture Collection (ATCC), Manassas, VA, USA. Ficoll-Paque 1077V R was purchased from Sigma-Aldrich Co. (St Louis, MO, USA). Blue coloring trypan was furnished by Nuclear (Sao Paulo, Brazil). Culture claw 25 cm^2 was obtained from Difco Laboratories (Detroit, MI, USA) and culture medium RPMI from Vitrocell (Sao Paulo, Brazil). All other chemicals were of analytical grade and were obtained from standard commercial suppliers.

2.2. Methods

2.2.1. Synthesis of Zirconia Nanoparticles

A total of 3.658 mL of $(C_4H_9O)_4Zr$ (Zirconium butoxide) was dissolved in 10 mL of CH_3COOH (acetic acid). The solution was hydrolyzed with 20 mL of deionized water, dropwise. A sol was formed within 15 min of hydrolysis with water, followed by continuous stirring. The formed sol was processed and gelated at 80 °C for 1 h, then dried at 100 °C to obtain powder samples. The calcination of the powder samples at 500 °C for 4 h led to the formation of ZrO_2 nanoparticles in accordance with past literature [16].

2.2.2. Synthesis of Ag_2O Nanoparticles

A total of 20 mL of deionized water was used to dissolve 3.398 g of silver nitrate. The solution was mixed with 1.92 g of citric acid that was previously dissolved in 10 mL of deionized water. The mixed solution was stirred for 15 min, non-stop, followed by the addition of ethylene glycol, dropwise, which served as a sol stabilizer while the stirring continued. The precipitate formed was washed with distilled water and dried at a temperature of 100 °C for 1 h. Ag_2O nanoparticles were obtained after the sample (obtained after calcination for 200 °C for 3 h) [17] was pulverized.

2.2.3. Synthesis of ZrO_2-Ag_2O Nanoparticles

A total of 3.658 mL of $(C_4H_9O)_4Zr$ (zirconium butoxide) was dissolved in 10 mL of CH_3COOH (acetic acid). The resulting mixture was hydrolyzed with 20 mL of deionized water, dropwise. An aqueous solution of $AgNO_3$ was later added to the mixture at different concentrations, of 0.1, 0.25, 0.5, 1.0, 2.0 mol/dm^3, with the samples denoted as Z-$A_{0.1}$, Z-$A_{0.25}$, Z-$A_{0.5}$, Z-$A_{1.0}$, and Z-$A_{2.0}$, respectively. During the reaction process, the concentration of $(C_4H_9O)_4Zr$ was maintained at 1 mol/dm^3 as the concentration of $AgNO_3$ was varied. A sol was formed from the solution and the sol was washed. The sol was placed in an oven for an 1 h for gelation to take place, and the sample was dried at 100 °C. After 4 h of calcination for 500 °C, ZrO_2-Ag_2O nanoparticles were formed [17].

2.3. Characterization

The phases of the synthesized nanoparticles were analyzed by X ray Diffraction (XRD), using an X'Pert PRO PANalytical instrument with Cu kα = 1.54056, 20 kV, with a scan from 5 to 80° at 2°/min scanning speed. Bruker Alpha-Platinum ATR instrument with 40 scans and resolution of 4 cm^{-1} measured between a wavelength of 4000 cm^{-1} and 400 cm^{-1} was used to determine the functional groups and the vibrational band of bonds. Cary100 spectrophotometer (Varian Corp. Meddelburg, Netherlands) was used to measure the UV–vis absorption spectra between the ranges of 100 and 900 nm at room temperature. The sizes of the nanoparticles were evaluated by dynamic light scattering (DLS) analysis in HORIBA SZ-100 Nanoparticle Analyzer (Horiba, Bensheim, Germany). Raman analysis was done with the WITec Raman spectrophotometer alpha300 R, having a confocal microscope system with a 532 nm laser; laser intensities varied between 0.649 and 9.538 W.cm^{-2} (focus spot of 700 µm), equipped with a 785 nm laser diode. The morphology of the nanoparticles and its components was observed with the aid of scanning transmission electron microscopy, with an energy-dispersive X-ray spectrometer (EDX) (STEM, JEOL JSM-6400, Milpitas, CA, USA) that was operated at 20 kV.

2.4. Antifungal Study

2.4.1. Disc Diffusion Method

The antifungal study of the synthesized nanoparticles was conducted by the disk diffusion method in accordance with the CLSI (2008). Four candida species, *C. albicans*, *C. dubliniensis*, *C. glabrata*, and *C. tropicalis* were cultured on Sabouraud Dextrose Agar (SDA) at 37 °C for 20 h; 100 µL of standardized suspensions of each fungi were placed on SDA. Each nanoparticle was prepared and measured before the inhibition zone tests. The nanoparticles were subsequently placed on the fungi culture plates. The agar plates were

incubated for 24 h at 37 °C. The antifungal effect was ascertained by taking measurements of the clear zones that corresponded to the inhibition formed around the nanoparticles using a vernier caliper instrument. The antifungal study for all of the fungi were done in triplicate.

2.4.2. Antifungal Susceptibility Testing

Before the test, isolates of *C. albicans*, *C. dubliniensis*, *C. glabrata,* and *C. tropicalis* were cultured on Sabouraud Dextrose Agar for a duration of 24 h at 37 °C. Broth microdilution methods were engaged for the antibiotic susceptibility testing of all the *Candida* species to analyze their susceptibilities to the synthesized ZrO_2, Ag_2O, and Z-A nanoparticles; this was done in accordance with the European Committee on Antimicrobial Susceptibility Testing (EUCAST). The suspension of the inoculum was prepared by putting four distinct colonies, with diameter sizes $\geq$1 mm in 3 mL of sterile distilled water, and was homogenized with a gyratory vortex mixer at a revolution of about 2000 rpm for 10 s. Variation of the cell density was conducted to match the 0.5 McFarland scale standard by making the appropriate dilution with the right amount of sterile distilled water. The standard suspension was diluted to obtain 1.3×10^6 CFU/mL, which served as the working suspension. The absorbance was recorded at a wavelength of 530 nm. The microdilution plates were plated with 0.02 mg of ZrO_2, Ag_2O, and Z-A nanoparticles. Thereafter, the plates were inoculated with 200 µL of freshly prepared suspension by adding the prepared yeast suspension to each well. The readings were taken after 24 h as the experiment was conducted in triplicate [18].

2.5. Oxidative Effects on Mononuclear Cells

2.5.1. Blood Collection

The sample used in this part of the analysis was peripheral human blood. The blood sample was obtained from the School Laboratory of Clinical Analyzes of Universidad Autonoma de Ciudad Juarez, Juarez, Mexico, in accordance with the guidelines and with the approval of the university's Ethics Committee for Research with Human Beings (Proyect: CIBE-2017-2-84). There is no identifying data associated with the obtained blood sample. Using a Vacutainer V R (BD Diagnostics, Plymouth, UK) and heparin tubes, and by venipunctures, human blood was collected from a healthy donor. The obtained human blood was separated into its constituents using Ficoll-Paque density gradient using 35 mL of blood samples. From the separated blood constituents, mononuclear cells were extracted. After separation, the viability of the mononuclear cells was determined.

2.5.2. Cell Viability

The extracted mononuclear cells were resuspended in RPMI-1640 at a calculated density of 1×10^6 cells/900 µL. A total of 50 µL each of the aliquot was measured into a 24-well plate (BD Falcon 352054, San Jose, CA, USA) and treated with 0.02 mg of ZrO_2, Ag_2O, and Z-A samples. The aliquot samples not exposed to the nanoparticles served as the control. The content in the 24-well plates were incubated for 24, 48, and 72 h in an incubator at 37 °C. Cell viability was determined after 24, 48, and 72 h of incubation, 5 µL of trypan blue was added to 40 µL of each of the samples. On completion of the addition process, each sample was analyzed with the FACSCAN flow cytometer. The results of cell viability were expressed in (%) and compared to the control. The extracted mononuclear cells were exposed in triplicate to ZrO_2, Ag_2O, and Z-A samples [19,20].

2.6. Statistical Analyses

All experimented assays were prepared and analyzed in three-fold, and all experiments were replicated at least three different times. The obtained results were presented as means $\pm$ standard deviation. Origin 9 was used for the t-test and one-way analysis of variance (ANOVA) was used, followed by post-hoc Tukey's tests for multiple comparisons. Values of $p \leq 0.05$ were taken as statistically significant.

3. Results

3.1. XRD, IR Analysis, and Zeta Potential Measurement

X-ray diffraction analysis was determined on all seven synthesized samples. The samples were measured on a clear amorphous glass substrate in the form of a thin powder film. The major 2Θ peak values illustrating the XRD crystalline patterns were at 24.6°, 28.6°, 31.9°, 35.4°, 50.6°, 55.8°, and 60.3°, which corresponded to the monoclinic phase of zirconia with a matching international standard file (JCPDS file no. 37-1484). The XRD crystalline patterns of Ag_2O had peaks that were designated to planes having hkl values, corresponding to 38.08° (111), 44.26° (200), 64.39° (220), and 77.36° (311), respectively, denoting the cubic silver oxide JCPDS No: 04-0783 (110). In the mixed samples of Z-A nanoparticles, a presence of peaks corresponded to peaks found in both ZrO_2 and Ag_2O nanoparticles. The absorption bands depicting the infrared spectrum of ZrO_2, Ag_2O, and Z-A samples were determined and previously reported [17]. From the reported IR analysis, Z-A samples showed absorption bands that were found within the fingerprint region, with the presence of the bands from 560 cm^{-1} to 760 cm^{-1}, with assignation to the metal-oxygen stretching mode because of the interatomic vibration. The presence of a band at 580 cm^{-1} assigned to the Ag-O bond confirmed the presence of Ag_2O; the presence of the characteristic absorption bands at 750, 680, and 480 cm^{-1} confirmed Zr-O bonds and were all reported. The zeta potential measurement was also reported among other characterizations that were carried out. It was reported that ZrO_2 nanoparticles confined stability on Ag_2O nanoparticles and this was responsible for the improved antimicrobial activity. The XRD, IR, and the zeta potential measurements were fully discussed with the diagrammatic representations of the spectra, included where applicable, and were recently published in literature [17].

3.2. UV-Visible Absorption Analysis

Optical absorption spectrum of size evolution is one of the characteristics of nanoparticles; therefore, with the use of UV-visible absorption spectroscopy, the optical characteristics of nanoparticles in the quantum size range was determined. UV-visible absorption spectra for ZrO_2, Ag_2O, and Z-A nanoparticles are presented in Figure 1 with the UV–visible absorption spectra of ZrO_2 and Ag_2O nanoparticles shown in Figure 1a. A strong and prominent absorption peak at about 300 nm was observed from the UV-visible absorption spectrum of zirconia nanoparticles (shown in Figure 1a) [21]. Ag_2O nanoparticles show a broad absorption in the UV-visible region (Figure 1a), which is in accordance with previous literature [22]. Figure 1b shows the UV-visible absorption spectra of Z-A nanoparticles with an absorption peak at 282 nm. From the UV-visible absorption spectra of Z-A nanoparticles, increasing the concentration of Ag_2O on ZrO_2 nanoparticles did not cause any change in the absorption peak. The absorption peak of the Z-A nanoparticles shows a shift to the lower wavelength due to the quantum confinement in samples when compared with that of ZrO_2 nanoparticles. This optical phenomenon presents the quantum size effect of these nanoparticles [23]. The UV-visible spectrum was measured within the range of 100 to 900 nm.

3.3. Raman Spectroscopy

Raman study was used to ascertain the interaction between ZrO_2 and Ag_2O nanoparticles and in conformity with the factor group theory, ZrO_2 has $18(9A_g + 9B_g)$ Raman active nodes, according to S. Rani et al. [24]. Figure 2a presents the Raman spectrum of ZrO_2 having the monoclinic peaks that corresponds to A_g at 530 cm^{-1}, B_g at 536 cm^{-1}, A_g at 545 cm^{-1}, A_g at 550 cm^{-1}, and A_g at 600 cm^{-1}. Figure 2b presents the Raman spectrum of Ag_2O nanoparticles showing bands at 548 cm^{-1} (sh), 565 cm^{-1}, 572 cm^{-1}, 580 cm^{-1}, and 610 cm^{-1}. A single Raman active vibration of T_{2g} symmetry at 565 cm^{-1} is the only predictive vibration expected of silver (I) oxide based on its symmetry considerations. The bands at 572 cm^{-1}, 580 cm^{-1}, and 610 cm^{-1} were assigned to silver carbonate that was formed due to the reaction of the oxide with carbon dioxide [25]. The presence of the band

corresponding to carbonate was due to the long exposure time of the nanoparticles to the atmosphere during the collection of the Raman data. In Figure 2c, Z-$A_{2.0}$ shows bands at 541 cm^{-1}, 545 cm^{-1}, 551 cm^{-1}, and 594 cm^{-1}. The observable shift from the bands of ZrO_2 and Ag_2O in the mixed sample of Z-$A_{2.0}$ confirms the interaction between ZrO_2 and Ag_2O.

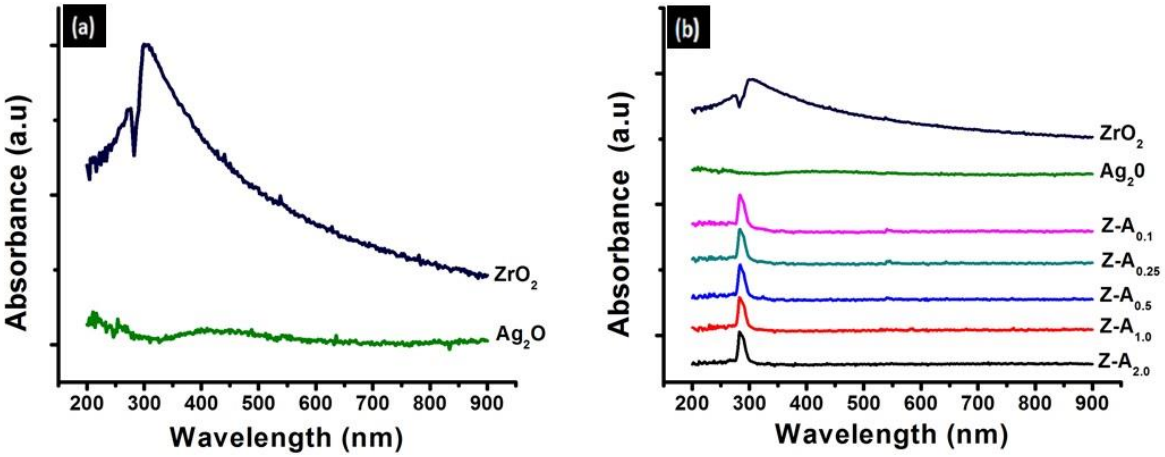

Figure 1. UV-visible absorption spectra of (**a**) ZrO_2 and Ag_2O (**b**) Z-A nanoparticles.

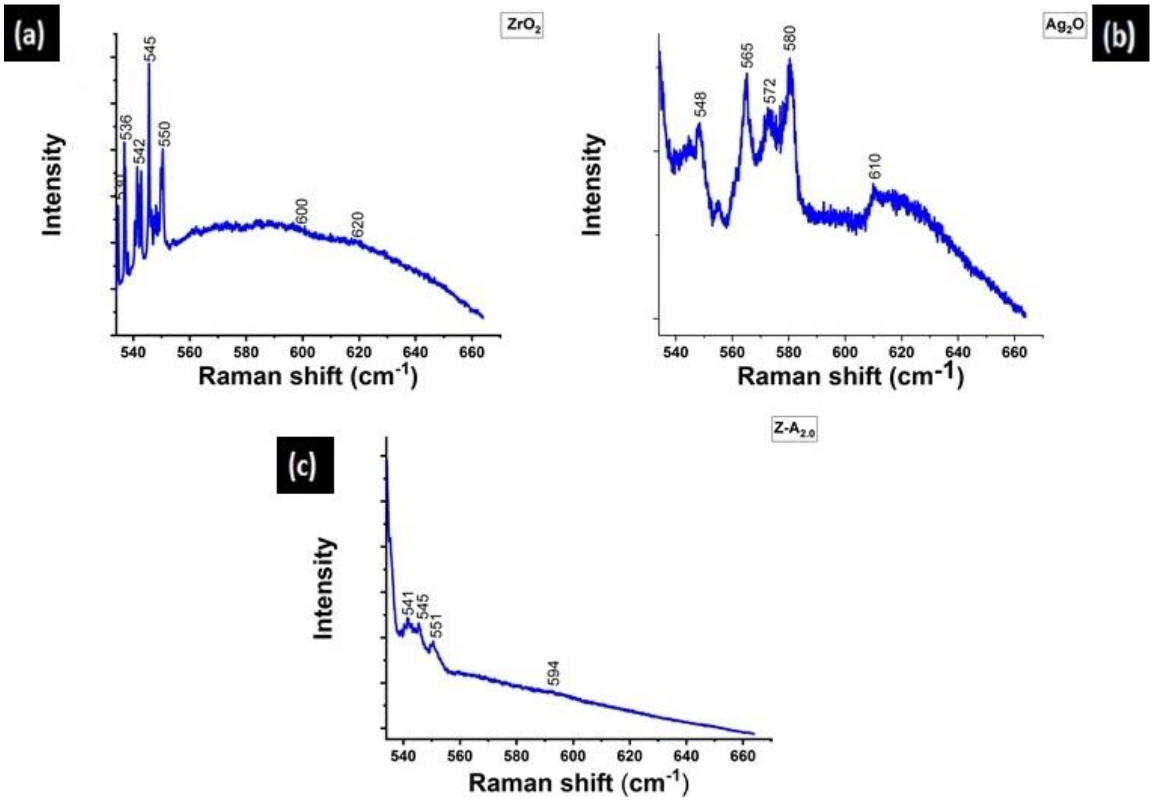

Figure 2. Raman spectra of (**a**) ZrO_2 (**b**) Ag_2O and (**c**) Z-$A_{2.0}$ nanoparticles.

3.4. Dynamic Light Scattering Analysis

The dynamic light scattering (DLS) analysis was used for the measurement of the size of the synthesized ZrO_2, Ag_2O, and Z-A nanoparticles in deionized water. Through laser beam illumination on suspension undergoing Brownian motion, DLS characterized the colloidal dispersion of nanomaterial [26]. The DLS results of ZrO_2, Ag_2O, Z-$A_{0.1}$, Z-$A_{0.25}$, Z-$A_{0.50}$, Z-$A_{1.0}$, and Z-$A_{2.0}$ nanoparticles in deionized water were 76 nm ± 2.4, 50 nm ± 3.2, 42 nm ± 2.2, 35 nm ± 1.8, 21 nm ± 1.0, 15 nm ± 1.5, and 14 nm ± 1.7, respectively.

3.5. Scanning Transmission Electron Microscopy

The morphology of the synthesized ZrO_2, Ag_2O, Z-$A_{0.5}$, and Z-$A_{2.0}$ nanoparticles was determined by scanning transmission electron microscopy (STEM) while the elemental constituent was determined by energy dispersive X-ray spectroscopy (EDX). The scanning transmission electron microscopy and the corresponding EDX images for elemental examination of ZrO_2, Ag_2O, Z-$A_{0.5}$, and Z-$A_{2.0}$ nanoparticles are presented in Figure 3a–h. To present a clearer picture, the STEM and EDX images of all the synthesized Z-A samples are not shown. Therefore, only representative samples were used for this analysis. In Figure 3a, the STEM image of ZrO_2 nanoparticles is spherical in shape and aggregated. The EDX image of ZrO_2 nanoparticles in Figure 3b shows the presence of zirconium and oxygen. The STEM image of Ag_2O nanoparticles shown in Figure 3c presents irregularly shaped nanoparticles with some agglomeration, while the EDX image of Ag_2O (Figure 3d) shows the presence of Ag and Oxygen. Figure 3e,g shows the STEM images of Z-$A_{0.5}$ and Z-$A_{2.0}$ with spherically shaped morphology with the nanoparticles of Z-$A_{2.0}$ highly dispersed. In Figure 3f,h, the EDX images shows the presence of zirconium, silver, and oxygen. The EDX image of each nanoparticle reveals the purity by showing the constituent that make up each sample. The carbon and aluminum presence in image d and f are due to the carbon tape used and the aluminum base support, respectively.

3.6. Antifungal Activity of Z-A Nanoparticles on *Candida* spp.

To analyze the data obtained from the antimicrobial experimental procedure, the inhibition zone around each applied nanoparticle was measured. From the results, it was observed that the mixed metal oxides of zirconium and silver recorded improved antimicrobial property when compared with the nanoparticles of only silver oxide or zirconium oxide. Z-$A_{2.0}$ nanoparticles showed the highest antimycotic activity against *C. albicans* followed by *C. glabrata*, *C. tropicalis,* and *C. dubliniensis*. From the combination effect of zirconium oxide with silver oxide, it was observed that the antimycotic activity increased as we increased the concentration of silver oxide against a fixed concentration of zirconia. The results of the inhibition zones are presented in Table 1.

Table 1. Zone of inhibition in (mm) formed on the different fungus by the different synthesized materials.

Materials	*C. albicans*	*C. dubliniensis*	*C. glabrata*	*C. tropicalis*
ZrO_2	0	0	0	0
Ag_2O	8.7 ± 0.6	6.3 ± 0.6	6.0 ± 1.0	8.0 ± 1.0
Z-$A_{0.1}$	9.0 ± 1.0	6.6 ± 1.0	6.3 ± 1.5	8.2 ± 1.5
Z-$A_{0.25}$	12.3 ± 0.6	7.3 ± 0.6	8.7 ± 2.5	8.7 ± 1.2
Z-$A_{0.5}$	13.3 ± 0.6	9.0 ± 1.0	10.3 ± 2.5	10.3 ± 0.6
Z-$A_{1.0}$	14.0 ± 1.0	10.7 ± 0.6	14.3 ± 1.5	13.7 ± 0.6
Z-$A_{2.0}$	18.3 ± 0.6	13.7 ± 1.5	17.0 ± 1.0	16.7 ± 0.6

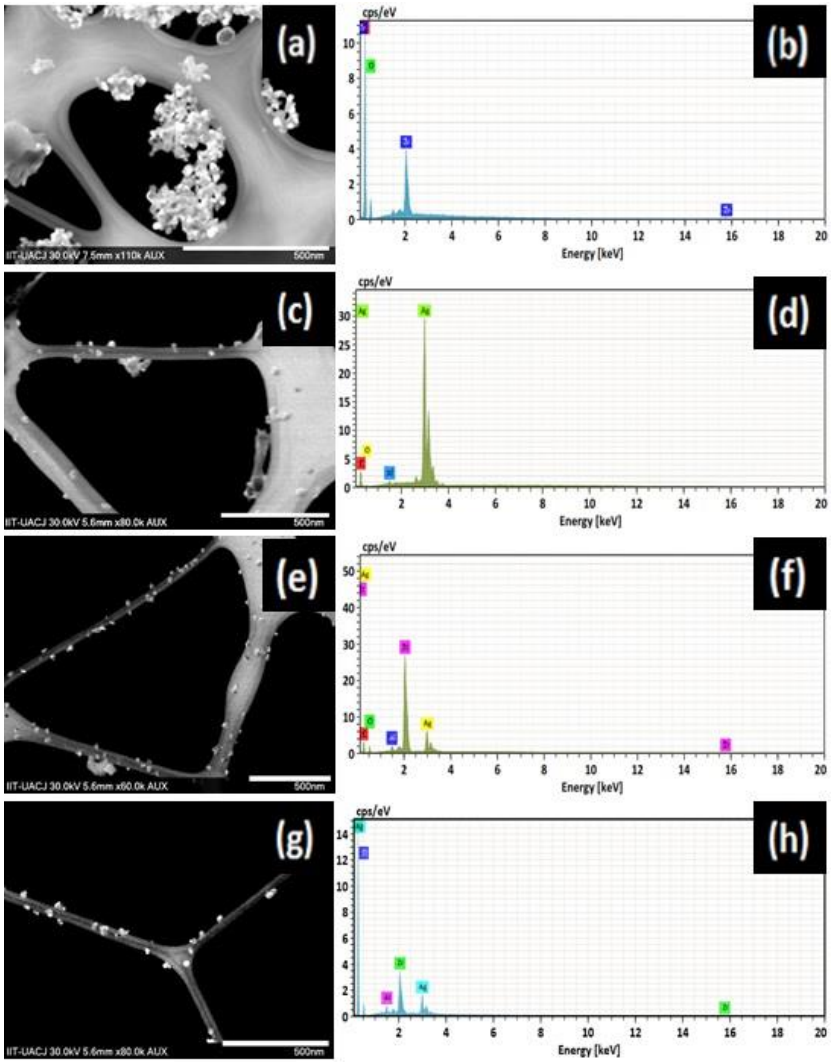

Figure 3. Scanning transmission electron microscope (STEM) and EDX images, respectively, of (**a**,**b**) ZrO_2, (**c**,**d**) Ag_2O, (**e**,**f**) Z-$A_{0.5}$, (**g**,**h**) Z-$A_{2.0}$.

3.7. Evaluation of the Growth Inhibition of Candida spp.

The antifungal activity of ZrO_2, Ag_2O, and Z-A nanoparticles was evaluated by monitoring the growth of the different *Candida* spp. (Figure 4) through the measurement of the variation in the optical density of each of the samples in a time rate of 24 h. The growth rate inhibition was measured from the time reliance of the noted growth of the tested *Candida* species. *Candida* species without the synthesized nanoparticles served as the control and showed a normal uninhibited pattern of growth during the 24 h test time. A strong sample dependent antimycotic activity was seen against all tested *Candida* species. The inhibition of the growth rate of *Candida* species by ZrO_2 nanoparticles that was recorded as a function of time shows a slight difference in the antimycotic activity of ZrO_2 nanoparticles when compared with the control (Figure 4). From Figure 4, the mixed metal oxide nanoparticles of Z-A show a stronger inhibition to all *Candida* species than pure ZrO_2 and Ag_2O nanoparticles. For emphasis, the inhibition of the growth rate caused by Z-$A_{0.25}$ on *Candida albicans* is stronger than the inhibition of the growth rate caused by Z-$A_{0.1}$. Across all tested fungal, it was observed that the higher the concentration of the Ag_2O against the fixed concentration of ZrO_2 nanoparticles, the stronger the inhibition effect, which in turn meant higher antifungal activity.

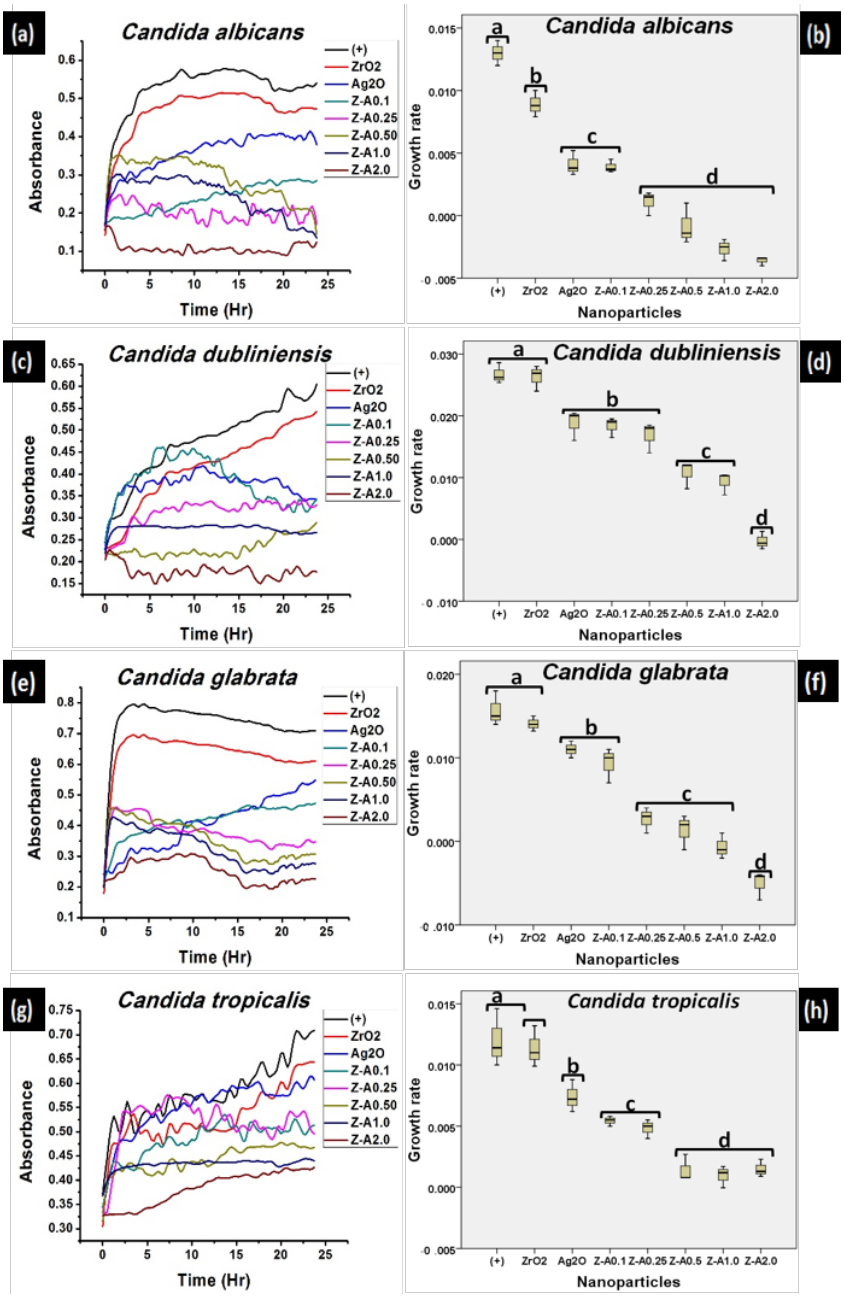

Figure 4. Growth kinetics and statistical computation respectively of (**a**,**b**) *C. albicans*, (**c**,**d**) *C. dubliniensis*, (**e**,**f**) *C. glabrata*, (**g**,**h**) *C. tropicalis* by ZrO_2, Ag_2O, and Z-A nanoparticles.

The mechanisms of action of the antifungal activities of Z-A nanoparticles can be accredited to the generation of reactive oxygen species, the result of the effect of Z-A nanoparticles to negatively disrupt the oxidative enzyme expression, which causes the inability of withstanding the resulting stress. Among other mechanisms of action of antifungal activities of Z-A nanoparticles is the upsetting of the antioxidant endogenic process, by unsettling the pathogen internal environment. In addition to the above-mentioned processes, the Z-A nanoparticles also lead to the alteration of the homeostatic redox reaction, and oxidative stress, which causes osmotic pressure imbalance, membrane destruction, and finally death [27]. From previous and related studies, Kim et al. investigated and reported

the process by which nanoparticles compromised the membrane permeability barrier of *Candida albicans* [28].

The turbidity of the media was observed at durations of 30 min at intervals to register the changes in the *Candida* species' growth rate. Figure 5 shows the percentage inhibition of each of the nanoparticles on each of the *Candida* species as computed from the microdilution analysis result. The obtained result shows only a small inhibition percentage of the *Candida* spp. at lower concentrations of Ag_2O against ZrO_2, but a much lower inhibition percentage for pure ZrO_2 and Ag_2O nanoparticles. There was an observable increase in the inhibition percentage as the concentration of Ag_2O against zirconia increased. At lower concentrations of Ag_2O against ZrO_2 (Z-$A_{0.1}$, Z-$A_{0.25}$, Z-$A_{0.5}$), the nanoparticles recorded lower inhibition percentage against all of the *Candida* spp. (Figure 5) when compared to the inhibition percentage recorded at higher concentrations of Ag_2O against ZrO_2 nanoparticles. All tested *Candida* spp. showed significant differences when compared to the control. From Figure 5, *Candida albicans* presented a 17% of inhibition for Z-$A_{0.1}$, which increased more than 5-fold to 97% in Z-$A_{2.0}$, with similar trends seen in other *Candida* spp. The sample-dependence analysis of the inhibition growth rate of *Candida* spp. showed that *Candida albicans* was the most susceptible to the inhibitory effect of the nanoparticles while *Candida tropicalis* was the least susceptible to Z-$A_{2.0}$. Z-$A_{2.0}$ recorded the highest inhibitory effect against all of the tested candida species as evaluated from the microdilution analysis.

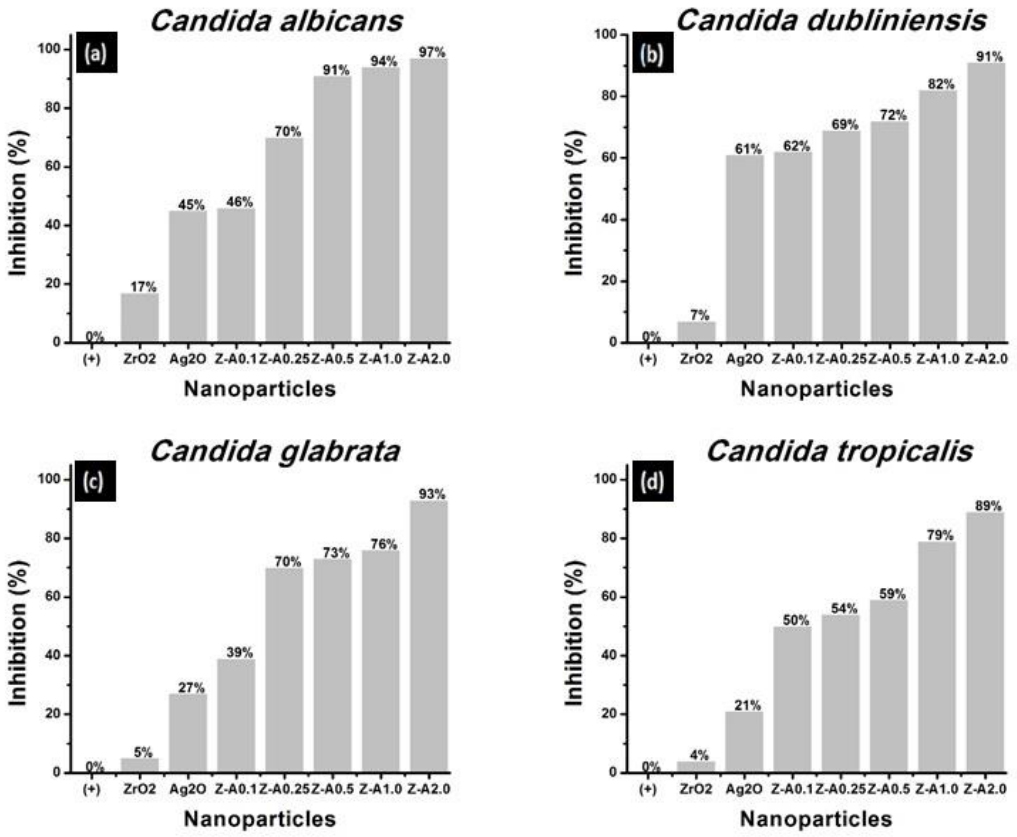

Figure 5. Comparison of the percentage inhibition of ZrO_2, Ag_2O, and Z-A nanoparticles against (**a**) *C. albicans*, (**b**) *C. dubliniensis*, (**c**) *C. glabrata*, (**d**) *C. tropicalis*.

3.8. Effect of Z-A Nanoparticle on Cell Viability

Peripheral blood mononuclear cells were exposed to Z-$A_{0.1}$, Z-$A_{0.50}$, and Z-$A_{2.0}$ for 24, 48, and 72 h. The peripheral blood mononuclear cells cultured without any of the synthesized nanoparticles functioned as the control (+) in this analysis and for all the tested

nanoparticles, the cell viability did not show any significant difference as a function of both time and concentration (Figure 6). For Z-$A_{0.1}$, Z-$A_{0.5}$, and Z-$A_{2.0}$, all of the nanoparticles produced near equivalent viability, both as a function of time and by virtue of the different samples that were tested. From previous literatures, the smaller the size, the larger the surface area to volume ratio, and the higher the toxicity of nanoparticles. The toxicity of nanoparticles increased as the size decreased [29]. Therefore, the objective here focused on comparing the toxic potentials of fixed concentrations of zirconia nanoparticles on mixing with different concentrations of Ag_2O (Z-$A_{0.1}$, Z-$A_{0.5}$, Z-$A_{2.0}$), on exposure to human mononuclear cells, a subset of immune cells that played a pivotal role against fungi pathogens [30]; moreover, on an ex vivo environment than can predict the in vivo response. Cell specific responses that take place because of variations in toxicity are caused by nanoparticles. In addition, the major determinant of intracellular responses and degree of cytotoxicity was dependent on the size of the nanoparticles and the target cell type [30]. From Figure 6, exposure of mononuclear cells (freshly isolated primary cells) to Z-$A_{0.1}$, Z-$A_{0.5}$, and Z-$A_{2.0}$ nanoparticles showed equal toxicity profiles for all of the tested nanoparticles in the time, and sample-dependent cytotoxicity, as shown by the cell viability assay. The equal toxicity profiles of all the tested nanoparticles observed in this study can be attributed to the non-toxic effect of ZrO_2 nanoparticles [31] imposed on Ag_2O nanoparticles.

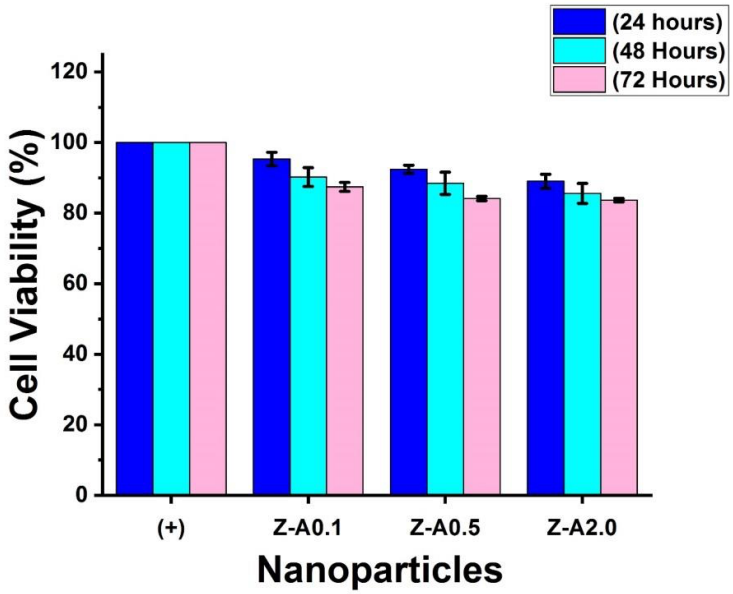

Figure 6. In vitro effect of Z-$A_{0.1}$, Z-$A_{0.5}$, and Z-$A_{2.0}$ nanoparticles on human peripheral blood mononuclear cells viability.

Table 2 shows the comparison of the inhibition zone formed on some of the tested fungi by the synthesized Z-$A_{2.0}$ nanoparticles from this study with those of the previously reported material. From the comparison, Z-$A_{2.0}$ nanoparticles showed superior antifungal activity when compared to other previously reported materials.

Table 2. Comparison of the zone of inhibition (mm) formed by different reported materials against some *Candida* spp. with the synthesized Z-$A_{2.0}$ nanoparticles.

Fungi	Material	Conc.	Inhibition Zone	References
C. albicans	Ag + *M. purpureus*	1 mM	16.7 ± 0.25	[32]
C. albicans	Ag-TiO_2	8.5% Ag	11	[33]
C. albicans	Ag	1 mM	10	[34]
C. albicans	Ag	80 µL	10	[35]
C. albicans	Z-$A_{2.0}$	1:2	18.3 ± 0.6	Present work
C. glabrata	Ag + *M. purpureus*	1 mM	18.7 ± 0.37	[32]
C. glabrata	Ag-TiO_2	8.5% Ag	15	[33]
C. glabrata	Ag	80 µL	9	[34]
C. glabrata	Z-$A_{2.0}$	1:2	17 ± 1.0	Present work
C. tropicalis	Ag + *M. purpureus*	1 mM	16.0 ± 0.44	[32]
C. tropicalis	Ag-TiO_2	8.5% Ag	15	[33]
C. tropicalis	Ag	1 mM	9	[34]
C. tropicalis	Ag	80 µL	9	[35]
C. tropicalis	Z-$A_{2.0}$	1:2	16.7 ± 0.6	Present work

4. Discussion

The results from the antifungal activity study reveal that mixed silver oxide with zirconia nanoparticles (Z-A) have better antifungal effect on all the *Candida* species than silver oxide and zirconia nanoparticles, based on the comparison of the result from the zone of inhibition (Table 1), growth kinetics (Figure 4), and the calculated percentage inhibition (Figure 5). Silver oxide nanoparticles stabilized by zirconia nanoparticles demonstrated pronounced antifungal activity because of their enhanced stability. This enhanced stability enables Z-A nanoparticles to disrupt the cell wall of the *Candida* spp. easily and, hence, increases their sensitivity to the activity of the mixed oxide nanoparticles. The highest antifungal activity of the mixed sample (Z-A) nanoparticles was recorded when zirconium oxide was mixed with 2 M concentration of silver oxide (Z-$A_{2.0}$). The results obtained from the zones of inhibition measurement (Table 1) show agreement to that obtained from microdilution analysis by virtue of the calculated percentage inhibition (Figure 5). The best antifungal activity was observed in the case of zirconia nanoparticle mixed with 2 M concentration of silver oxide (Z-$A_{2.0}$), and particularly against *Candida albicans* and *Candida glabrata*. Unlike the pure zirconia and silver oxide nanoparticles, the Z-A mixed samples recorded high values for zone of inhibition, increasing from 9.0 mM to 18.3 mM, and a high percentage of inhibition from 46% to 97% in the case of *C. albicans*. The observed increase in the inhibition zone and inhibition percentage result from the improved antifungal activity of silver oxide nanoparticles due to the stabilizing effect of zirconia nanoparticles.

The improved antifungal activity of Z-A nanoparticles is a result of the antifungal effect of silver oxide nanoparticles coupled with the stabilizing effect of zirconia nanoparticles. The permeability of the cell wall and the cytoplasmic membrane is penetrated by Z-A nanoparticles by bonding with lipids and proteins. The presence of Z-A nanoparticles in the cell leads to toxic effect. After Z-A nanoparticles have disrupted the cell wall and cytoplasmic membrane that lead to cell lysis, it furthers its actions by inhibiting enzymatic activity of various enzymes, such as the activity of ATPase in P-glycoprotein or the activity of transferase in lecithin [36]. By having a comparative study between the antifungal activity of ionic silver and the synthesized Z-A nanoparticles from this work, it was reported that, despite the antifungal activity recorded by ionic silver, it proved to be highly cytotoxic to eukaryotic cell lines, as shown by the cytotoxicity assay from a previous study [37]. However, Z-A nanoparticles did not show any cytotoxic effects to human mononuclear cells at the concentrations at which it was synthesized (Figure 6).

5. Conclusions

Many researchers reported that synthesis of pure silver nanoparticles agglomerate and show cytotoxic behavior. In contrast, synthesis of mixed metal oxide nanoparticles, in

which silver nanoparticles are mixed with zirconia nanoparticles, preventing agglomeration of nanoparticles, was carried out. In this study, the synthesis of mixed metal oxide nanoparticles of silver and zirconia was reported. The Z-A nanoparticles had significant antifungal activities and were potent in inhibiting the growth and the pathogenicity of the *Candida* species. The inhibitory potency was attributed to the destruction of the integrity of the cell wall and the lack of cell toxicity was attributed to the non-toxic effect of zirconia that was conferred on silver oxide.

Author Contributions: Conceptualization, A.P.A. and S.Y.R.-L.; methodology, A.P.A. and S.Y.R.-L.; software, A.P.A.; validation, A.P.A. and S.Y.R.-L.; formal analysis, A.P.A. and S.Y.R.-L.; investigation, A.P.A., B.L.E.-C. and S.Y.R.-L.; resources, A.P.A., B.L.E.-C. and S.Y.R.-L.; data curation, A.P.A. and S.Y.R.-L.; writing—original draft preparation, A.P.A. and S.Y.R.-L.; writing—review and editing, A.P.A. and S.Y.R.-L.; visualization, A.P.A. and S.Y.R.-L.; supervision, S.Y.R.-L.; project administration, A.P.A. and S.Y.R.-L.; funding acquisition, B.L.E.-C. and S.Y.R.-L. All authors have read and agreed to the published version of the manuscript.

Funding: This research received no external funding.

Institutional Review Board Statement: The study was conducted according to the guidelines of the Declaration of Mexico and approved by the Institutional Animal Care and Use Committee (IACUC), Comite Institucional de Etica y Bioetica, Universidad Autonoma de Ciudad Juarez (CIEB-UACJ) and the NOM-062-ZOO-1999 on technical specifications for the production, care and use of laboratory animals during the entire process of the experimental phase (Proyect: CIBE-2017-2-84, Date: 23 October 2017).

Informed Consent Statement: Informed consent was obtained from all subjects involved in the study.

Data Availability Statement: The study did not report any data.

Acknowledgments: Thanks to PRODEP, Universidad Autónoma de Ciudad Juárez and CONACYT.

Conflicts of Interest: The authors declare no conflict of interest.

References

1. Artunduaga Bonilla, J.J.; Paredes Guerrero, D.J.; Sánchez Suárez, C.I.; Ortiz López, C.C.; Torres Sáez, R.G. In vitro antifungal activity of silver nanoparticles against fluconazole-resistant Candida species. *World J. Microbiol. Biotechnol.* **2015**, *31*, 1801–1809. [CrossRef]
2. Owaid, M.N.; Raman, J.; Lakshmanan, H.; Al-Saeedi, S.S.S.; Sabaratnam, V.; Ali Abed, I. Mycosynthesis of silver nanoparticles by Pleurotus cornucopiae var. citrinopileatus and its inhibitory effects against Candida sp. *Mater. Lett.* **2015**, *153*, 186–190. [CrossRef]
3. De Castro, R.D.; de Souza, T.M.P.A.; Bezerra, L.M.D.; Ferreira, G.L.S.; de Brito Costa, E.M.M.; Cavalcanti, A.L. Antifungal activity and mode of action of thymol and its synergism with nystatin against Candida species involved with infections in the oral cavity: An in vitro study. *BMC Complement. Altern. Med.* **2015**, *15*, 1–7. [CrossRef]
4. Naglik, J.R.; Moyes, D.L.; Wächtler, B.; Hube, B. Candida albicans interactions with epithelial cells and mucosal immunity. *Microbes Infect.* **2011**, *13*, 963–976. [CrossRef]
5. Bondaryk, M.; Kurzątkowski, W.; Staniszewska, M. Antifungal agents commonly used in the superficial and mucosal candidiasis treatment: Mode of action and resistance development. *Postep. Dermatol. Alergol.* **2013**, *30*, 293–301. [CrossRef]
6. Perween, N.; Khan, H.M.; Fatima, N. Silver nanoparticles: An upcoming therapeutic agent for the resistant Candida infections. *J. Microbiol. Exp.* **2019**, *7*, 49–54. [CrossRef]
7. Brayner, R.; Dahoumane, S.A.; Yéprémian, C.; Djediat, C.; Meyer, M.; Couté, A.; Fiévet, F. ZnO nanoparticles: Synthesis, characterization, and ecotoxicological studies. *Langmuir* **2010**, *26*, 6522–6528. [CrossRef]
8. Gutiérrez, J.A.; Caballero, S.; Díaz, L.A.; Guerrero, M.A.; Ruiz, J.; Ortiz, C.C. High Antifungal Activity against Candida Species of Monometallic and Bimetallic Nanoparticles Synthesized in Nanoreactors. *ACS Biomater. Sci. Eng.* **2018**, *4*, 647–653. [CrossRef] [PubMed]
9. Vivekanandhan, S.; Christensen, L.; Misra, M.; Kumar Mohanty, A. Green Process for Impregnation of Silver Nanoparticles into Microcrystalline Cellulose and Their Antimicrobial Bionanocomposite Films. *J. Biomater. Nanobiotechnol.* **2012**, *3*, 371–376. [CrossRef]
10. Sundeep, D.; Vijaya Kumar, T.; Rao, P.S.S.; Ravikumar, R.V.S.S.N.; Gopala Krishna, A. Green synthesis and characterization of Ag nanoparticles from Mangifera indica leaves for dental restoration and antibacterial applications. *Prog. Biomater.* **2017**, *6*, 57–66. [CrossRef] [PubMed]

11. Singh, S.P.; Bhargava, C.S.; Dubey, V.; Mishra, A.; Singh, Y. Silver nanoparticles: Biomedical applications, toxicity, and safety issues. *Int. J. Res. Pharm. Pharm. Sci.* **2017**, *2*, 2455–2698.
12. Gowri, S.; Rajiv Gandhi, R.; Sundrarajan, M. Structural, optical, antibacterial and antifungal properties of zirconia nanoparticles by biobased protocol. *J. Mater. Sci. Technol.* **2014**, *30*, 782–790. [CrossRef]
13. Ayanwale, A.P.; Cornejo, A.D.; González, J.C.C.; Cristóbal, L.F.E.; López, S.Y.R. Review of the Synthesis, Characterization and Application of Zirconia Mixed Metal Oxide Nanoparticles. *Int. J. Res. Granthaalayah* **2018**, *6*, 136–145. [CrossRef]
14. Karn-Orachai, K.; Sakamoto, K.; Laocharoensuk, R.; Bamrungsap, S.; Dharakul, T.; Miki, K. SERS-based immunoassay on 2D-arrays of Au@Ag core-shell nanoparticles: Influence of the sizes of the SERS probe and sandwich immunocomplex on the sensitivity. *RSC Adv.* **2017**, *7*, 14099–14106. [CrossRef]
15. Panáček, A.; Kolář, M.; Večeřová, R.; Prucek, R.; Soukupová, J.; Kryštof, V.; Hamal, P.; Zbořil, R.; Kvítek, L. Antifungal activity of silver nanoparticles against Candida spp. *Biomaterials* **2009**, *30*, 6333–6340. [CrossRef] [PubMed]
16. Precious Ayanwale, A.; Reyes-López, S.Y. ZrO2-ZnO Nanoparticles as Antibacterial Agents. *ACS Omega* **2019**, *4*, 19216–19224. [CrossRef]
17. Ayanwale, A.P.; Ruíz-Baltazar, A. de J.; Espinoza-Cristóbal, L.; Reyes-López, S.Y. Bactericidal Activity Study of ZrO_2-Ag_2O Nanoparticles. *Dose-Response* **2020**, *18*, 1–13. [CrossRef]
18. Muñoz-Escobar, A.; Reyes-López, S.Y. Antifungal susceptibility of Candida species to copper oxide nanoparticles on polycaprolactone fibers (PCL-CuONPs). *PLoS ONE* **2020**, *15*, e0228864. [CrossRef]
19. Mota Ferreira, L.; Gehrcke, M.; Ferrari Cervi, V.; Eliete Rodrigues Bitencourt, P.; Ferreira da Silveira, E.; Hofstatter Azambuja, J.; Prates Ramos, A.; Nascimento, K.; Beatriz Moretto, M.; Braganhol, E.; et al. Pomegranate seed oil nanoemulsions with selective antiglioma activity: Optimization and evaluation of cytotoxicity, genotoxicity and oxidative effects on mononuclear cells. *Pharm. Biol.* **2016**, *54*, 2968–2977. [CrossRef]
20. Mendoza, A.; Torres-Hernandez, J.A.; Ault, J.G.; Pedersen-Lane, J.H.; Gao, D.; Lawrence, D.A. Silica nanoparticles induce oxidative stress and inflammation of human peripheral blood mononuclear cells. *Cell Stress Chaperones* **2014**, *19*, 777–790. [CrossRef]
21. Kumaresan, M.; Vijai Anand, K.; Govindaraju, K.; Tamilselvan, S.; Ganesh Kumar, V. Seaweed Sargassum wightii mediated preparation of zirconia (ZrO_2) nanoparticles and their antibacterial activity against gram positive and gram negative bacteria. *Microb. Pathog.* **2018**, *124*, 311–315. [CrossRef] [PubMed]
22. Zhang, J.; Liu, H.; Ma, Z. Flower-like Ag_2O/Bi_2MoO_6 p-n heterojunction with enhanced photocatalytic activity under visible light irradiation. *J. Mol. Catal. A Chem.* **2016**, *424*, 37–44. [CrossRef]
23. Negahdary, M.; Habibi-Tamijani, A.; Asadi, A.; Ayati, S. Synthesis of zirconia nanoparticles and their ameliorative roles as additives concrete structures. *J. Chem.* **2013**, *2013*, 314862. [CrossRef]
24. Rani, S.; Aggarwal, M.; Kumar, M.; Sharma, S.; Kumar, D. Removal of methylene blue and rhodamine B from water by zirconium oxide/graphene. *Water Sci.* **2016**, *30*, 51–60. [CrossRef]
25. Waterhouse, G.I.N.; Bowmaker, G.A.; Metson, J.B. The thermal decomposition of silver (I, III) oxide: A combined XRD, FT-IR and Raman spectroscopic study. *Phys. Chem. Chem. Phys.* **2001**, *3*, 3838–3845. [CrossRef]
26. Gurunathan, S.; Jeong, J.K.; Han, J.W.; Zhang, X.F.; Park, J.H.; Kim, J.H. Multidimensional effects of biologically synthesized silver nanoparticles in Helicobacter pylori, Helicobacter felis, and human lung (L132) and lung carcinoma A549 cells. *Nanoscale Res. Lett.* **2015**, *10*, 1–17. [CrossRef]
27. Kumari, M.; Giri, V.P.; Pandey, S.; Kumar, M.; Katiyar, R.; Nautiyal, C.S.; Mishra, A. An insight into the mechanism of antifungal activity of biogenic nanoparticles than their chemical counterparts. *Pestic. Biochem. Physiol.* **2019**, *157*, 45–52. [CrossRef]
28. Kim, K.J.; Sung, W.S.; Suh, B.K.; Moon, S.K.; Choi, J.S.; Kim, J.G.; Lee, D.G. Antifungal activity and mode of action of silver nano-particles on Candida albicans. *Biometals* **2009**, *22*, 235–242. [CrossRef]
29. Stankic, S.; Suman, S.; Haque, F.; Vidic, J. Pure and multi metal oxide nanoparticles: Synthesis, antibacterial and cytotoxic properties. *J. Nanobiotechnol.* **2016**, *14*, 73. [CrossRef]
30. Sahu, D.; Kannan, G.M.; Tailang, M.; Vijayaraghavan, R. In Vitro Cytotoxicity of Nanoparticles: A Comparison between Particle Size and Cell Type. *J. Nanosci.* **2016**, *2016*, 1–9. [CrossRef]
31. Babu, M.M.; Prasad, P.S.; Bindu, S.H.; Venkateswara Rao, P.; Govindan, N.P.; Veeraiah, N.; Özcan, M. Bioactivity, antibacterial activity and functionality of zirconia doped zinc phosphate bioglasses for application in dentistry. *Mater. Sci. Eng. C* **2020**, *114*, 111052. [CrossRef]
32. El-Baz, A.F.; El-Batal, A.I.; Abomosalam, F.M.; Tayel, A.A.; Shetaia, Y.M.; Yang, S.T. Extracellular biosynthesis of anti-Candida silver nanoparticles using Monascus purpureus. *J. Basic Microbiol.* **2016**, *56*, 531–540. [CrossRef]
33. Zielińska, A.; Kowalska, E.; Sobczak, J.W.; Łacka, I.; Gazda, M.; Ohtani, B.; Hupka, J.; Zaleska, A. Silver-doped TiO_2 prepared by microemulsion method: Surface properties, bio- and photoactivity. *Sep. Purif. Technol.* **2010**, *72*, 309–318. [CrossRef]
34. Rajamanickam, K.; Sudha, S.S.; Francis, M.; Sowmya, T.; Rengaramanujam, J.; Sivalingam, P.; Prabakar, K. Microalgae associated Brevundimonas sp. MSK 4 as the nano particle synthesizing unit to produce antimicrobial silver nanoparticles. *Spectrochim. Acta Part A Mol. Biomol. Spectrosc.* **2013**, *113*, 10–14. [CrossRef] [PubMed]
35. Khan, N.T.; Mushtaq, M. Determination of Antifungal Activity of Silver Nanoparticles Produced from Aspergillus niger. *Biol. Med.* **2016**, *9*, 1–4. [CrossRef]

36. Fernández, E.; Benito, J.M.; Pazos, C.; Coca, J. Ceramic membrane ultrafiltration of anionic and nonionic surfactant solutions. *J. Memb. Sci.* **2005**, *246*, 1–6. [CrossRef]
37. Kvitek, L.; Vanickova, M.; Panacek, A.; Soukupov, J.; Dittrich, M.; Valentova, E.; Prucek, R.; Bancirova, M.; Milde, D.; Zboril, R. Initial study on the toxicity of silver nanoparticles (NPs) against Paramecium caudatum. *J. Phys. Chem. C* **2009**, *113*, 4296–4300. [CrossRef]